In toto live imaging in scuttle fly *Megaselia abdita* reveals transitions towards a novel extraembryonic architecture.

Francesca Caroti[1,4], Everado González Avalos[1]*, Paula González Avalos[1]*, Dimitri Kromm[2,3], Viola Noeske[1], Maike Wosch[1], Lucas Schütz[1], Lars Hufnagel[2], Steffen Lemke[1]

[1] Centre for Organismal Studies Heidelberg (COS), Im Neuenheimer Feld 230, 69120 Heidelberg, Germany
[2] European Molecular Biology Laboratory (EMBL), Meyerhofstraße 1, 69117 Heidelberg, Germany
[3] Heidelberg University, Faculty of Biosciences, Im Neuenheimer Feld 234, 69120 Heidelberg, Germany
[4] current address: Centre of Microbial and Plant Genetics, Kasteelpark Arenberg 20, 3001 Leuven, Belgium
* equal contribution

Corresponding author: steffen.lemke@cos.uni-heidelberg.de

ABSTRACT

Evolutionary novelty can be generally traced back to continuous changes rather than disruptive transformations, yet the sudden appearance of novel developmental traits is not well understood. Here we use the extraembryonic amnioserosa in *Drosophila melanogaster* as example for a suddenly and newly evolved epithelium, and we ask how this tissue originated by gradual transitions from its two ancestors, amnion and serosa. To address this question, we used *in toto* time-lapse recordings to analyze an intermediate mode of extraembryonic development in the scuttle fly *Megaselia abdita*. Our results suggest that the amnioserosa evolved by loss of serosa spreading without disrupting the developmental programs of serosa and amnion. Our findings imply that the Drosophila amnioserosa has retained properties of the ancient serosa and, more generally, indicate that non-autonomous interactions between tissues can be a compelling variable for the evolution of epithelial properties.

Impact Statement

The Drosophila amnioserosa originated as a composite extraembryonic epithelium by loss of epithelial spreading and rather than changes in amnion or serosa tissue differentiation.

Keywords

Megaselia abdita, extraembryonic tissue (amnion / serosa), *in toto* time-lapse recording, epithelial morphogenesis, tissue spreading, evolution of development

INTRODUCTION

At the macroscopic level, even the most sudden appearance of novel structures and animal traits is a result of continuous gradual changes, which can be traced back to deep conservation through missing link fossils (Darwin, 1872; Shubin et al., 2006; Xu et al., 2011). At the microscopic level of cells and tissues in the developing organism, the abrupt origin of novel structures and properties is less well understood. To systematically explore how successive evolutionary transitions cumulatively lead to the origin of novel epithelial structure and function, recent work has established extraembryonic development in insects as model for experimental evolution (Hallgrímsson et al., 2012; Horn et al., 2015; Schmidt-Ott and Kwan, 2016). Here we study the evolutionary history of a recent extraembryonic innovation in flies and show how it originated by gradual and cumulative transitions from deeply conserved structures.

Extraembryonic development in insects begins prior to the onset of gastrulation, when distinct areas of the blastula are set aside to contribute to either the embryo or extra-embryonic epithelia (Anderson, 1972a; Anderson, 1972b). In most insects, the so-called blastoderm embryo is molecularly patterned to give rise to two extra-embryonic epithelia, the amnion and the serosa (Horn et al., 2015; Schmidt-Ott and Kwan, 2016). The subsequent and overall insect-typical development of amnion and serosa has been exemplarily documented in the beetle *Tribolium castaneum*. In *T.castaneum*, the serosa is formed from a population of cells in the anterodorsal blastoderm (van der Zee et al., 2005; van der Zee et al., 2006). With the onset of gastrulation, the cells of this serosa anlage spread uniformly over the embryo and engulf it completely by the end of gastrulation (Benton et al., 2013; Handel et al., 2000; van der Zee et al., 2005). The amnion is specified in a circumferential ring next to the serosa (Benton, 2017; van der Zee et al., 2005); as the serosa spreads over the embryo, the amnion folds underneath, spreads between serosa and embryo, and eventually covers the posteroventral side of the embryo (Benton, 2017; Benton et al., 2013; Handel et al., 2000; van der Zee et al., 2005).

In contrast to most other insects, the fruit fly *Drosophila melanogaster* develops a single extraembryonic tissue, the amnioserosa (Campos-Ortega and Hartenstein, 1997). The amnioserosa is specified within the dorsal blastoderm; with the onset of gastrulation, amnioserosa cells flatten and the extraembryonic tissue spreads in between the extending domains of the developing embryo (Campos-Ortega and Hartenstein, 1997). Cell shape changes in the amnioserosa are active and occur independently of other nearby morphogenetic activity (Pope and Harris, 2008). In contrast to the serosa, however, the amnioserosa does not fold over the embryo, it remains exclusively on the dorsal side, and a distinct ventral amnion does not form.

An intermediate mode of extraembryonic tissue formation has been described for the group of lower cyclorrhaphan flies like phorids and syrphids (Rafiqi et al., 2008). This intermediate mode may serve as missing link between ancestral extraembryonic development similar to amnion and serosa formation in *T.castaneum* today, and the derived mode of amnioserosa formation described for *D.melanogaster*. Characteristic for this intermediate mode is the formation of a complete serosa and absence of a ventrally closed amnion. The development of both tissues has been exemplarily analyzed in the phorid *Megaselia abdita* (Rafiqi et al., 2008; Rafiqi et al., 2010; Rafiqi et al., 2012). In *M.abdita*, serosa and amnion are both set up by molecular patterning in the dorsal blastoderm embryo (Kwan et al., 2016). Previous analyses of their subsequent development concluded that the amnioserosa evolved from

ancestral serosa and amnion in two major transitions (Rafiqi et al., 2008; Schmidt-Ott and Kwan, 2016). Based on functional analyses of gene regulation and expression, the first transition from ancestral to intermediate mode of extraembryonic development mostly affected amnion morphogenesis. Here, amnion formation changed from being linked to serosa expansion and topologically located on the ventral side of the embryo to expanding autonomously and being located on the dorsal side of the embryo. The second transition from intermediate to derived mostly affected serosa differentiation. Here, the serosa changed from being a stably defined character throughout development to becoming a transitory tissue that transdifferentiates into a dorsal amnion midway through embryogenesis. Both of these transitions invoke major remodeling of amnion and serosa properties very upstream in development, which seems to collide with the concept of gradual and continuous changes that underlie the origin of macroscopic novelty.

To test whether the amnioserosa could have evolved without invoking major remodeling in the developmental programs of amnion and serosa, we aimed to identify a minimal set of changes that could provide continuous links from ancestral to intermediate, and from intermediate to derived mode of extraembryonic tissue formation. This approach required us to measure and compare dynamic cell and tissue properties of the participating epithelia, and we established single plane illumination microscopy (SPIM) to quantify these properties at high spatiotemporal resolution in *M.abdita*. Based on our SPIM recordings, we revealed and tracked extraembryonic tissue differentiation and spreading. Analyses of amnion morphogenesis demonstrate that the Megaselia amnion is located on the ventral side of the embryo, very similar to what has been described for Tribolium. Analyses of serosa morphogenesis show that the tissue is actively expanding. We observed cell and tissue oscillation in the serosa in areas where the tissue was in contact with the underlying yolk sac. We did not detect such oscillations in the Megaselia amnion but in the Drosophila amnioserosa, which we found to share additional and independent properties with the Megaselia serosa. We propose that the amnioserosa originated as a composite tissue and evolved in two gradual transitions from a ventral amnion and complete serosa, first by loss of ventral amnion fusion, and second by loss of serosa spreading in response to genetic changes in the yolk sac.

RESULTS

To be able to compare amnion and serosa cell and tissue properties in *M.abdita* with extraembryonic epithelia of other species, we first asked whether differences in cell shape of fixed embryos were sufficient to characterize amnion and serosa development. *M.abdita* embryos were fixed at three subsequent stages of development, and the cell outline was revealed by staining filamentous actin (F-actin). Cell height, apical area, and apical roundness (circularity) were measured at various positions along the anterior-posterior axis and the embryonic circumference (i) in the blastoderm before the onset of gastrulation, (ii) after germband extension and the initial formation of a dorsal extraembryonic tissue, (iii) during or briefly after detachment of the serosa (Figure 1). During blastoderm stage, all cells appeared to be tall and equal in size, shape, and volume (Figure 1A-Ab). After the onset of germband extension but prior to detachment of the serosa, two classes of cells appeared to be qualitatively distinguishable based on differences in cell shape: cells of the lateral region of the embryo were characterized by a slight decrease in cell height but maintained apical

area and circularity, while cells along the dorsal midline appeared flattened and stretched, and deviated from the ideal circular apex (Figure 1B-Bb'). Similarly, during or briefly after detachment of the serosa, cell shapes were observed to fall into two qualitatively distinct classes, i.e. tall cells with a round apex and a small apical area, and thin cells with a stretched and flat cell area (Figure 1C-Cb').

To address the extent at which each individual parameter contributed to the global differences in cell shape between embryonic and serosa as well as amnion tissue spreading, we performed a principal component analysis of all recorded stages, cells, and parameters (Figure 1 D-G). Notably, the first two principal components permitted the full discrimination between blastoderm and embryonic cells on the one hand and extraembryonic cells on the other. However, for all of the analyzed stages they did not provide support for two classes of distinctly spreading extraembryonic tissues, suggesting that amnion and serosa cells changed their shape very similarly or that differences in their dynamic properties were lost by our analyses in fixed tissue.

Tracked cell dynamics allow to distinguish serosal and amniotic properties

To test whether amnion and serosa could be distinguished through their dynamics during early extraembryonic development, we reasoned that cells would need to be tracked several hours from a dorsolateral position to a position along the ventral midline. To reveal and characterize the dynamics of extraembryonic cells globally and in long-term time-lapse recordings, we established injection of recombinant Lifeact-mCherry protein as means to instantaneously mark F-actin *in vivo*, and we recorded development from the onset of gastrulation until the end of germband retraction using *in toto* imaging under low phototoxic burden with a selected plane illumination microscope (SPIM, Figure 2). We found embryonic development in Megaselia as imaged by SPIM to be overall reproducible and major dynamics of the extending and retracting germband could be aligned between embryos without substantial variance (Figure 2 – figure supplement 1). To visualize and track cells all around the embryo, we obtained a two-dimensional representation of the embryo surface by using cylindrical projections (Material and Methods).

Based on this approach, we analyzed the expanding extraembryonic tissues at the lateral side of the embryo as example (Figure 2A). Serosa cells could be identified and distinguished from non-serosal extraembryonic cells based on their unique ability to spread over adjacent cell layers (Figure 2B-C'). Based on cells tracked on either side of the embryo, serosa development started from tall, columnar cells along the dorsal midline. This blastoderm anlage for the serosa was determined to be about six to seven cells wide (Figure 2D), which coincided with expression of the homeodomain transcription factor zerknüllt (zen) (Figure 2E) and is consistent with previous genetic analyses (Rafiqi et al., 2008; Rafiqi et al., 2010; Rafiqi et al., 2012).

Immediately next to the serosa we observed several rows of intermediate sized cells (Figure 2F), which were eventually overgrown by the expanding serosa (Figure 2G). Based on long-term tracking, we identified two distinct populations among these intermediate sized cells. The single row of cells in direct contact with the serosa originated from a one-cell wide

domain immediately adjacent to the serosa anlage (Figure 2H). These cells did not divide (Figure 2I) and retained their apical cell size for an extended period of time (Figure 2J). All other intermediate sized cells eventually divided and decreased their apical cell area shortly after germband extension (Figure 2G-J). Based on these differences, we interpreted the cells next to the serosa as amnion, and the remaining cells as temporarily enlarged ectodermal cells. We find this interpretation consistent with previous genetic models, which used a gap of gene expression to predict that the Megaselia amnion was specified in a small domain directly adjacent to the serosa (Kwan et al., 2016; Rafiqi et al., 2012). According to our measures, serosa cells were about three times as large as amnion cells prior to separation from the amnion; following the separation, the apical cell area of serosa cells increased further and resulted in cells that were 10-20 times larger than amnion cells (Figure 2J).

To test whether our amnion cell tracking was robust, we asked whether we could clarify the existence of an anterior amnion in *M.abdita*. For this, we tracked cells of the extraembryonic anlage anterior of the cephalic furrow (Figure 2K). We found that by about 55% germband extension, all cells had moved posterior to the cephalic furrow and spread laterally, indicating that cells that defined lateral serosa and amnion in the blastoderm had rearranged to form the broad leading edge for the anterior front of the expanding extraembryonic tissue (Figure 2L).

The amnion forms a ventrally open epithelium

To identify the minimal changes in amnion morphogenesis that could explain the transition from ancestral to intermediate extraembryonic development represented in *M.abdita*, we used our *in toto* time-lapse recordings to visualize the dynamics of Megaselia amnion morphogenesis. We first used image processing to digitally “peel off” the serosa and then tracked individual amnion cells and their position along the embryonic circumference (Figure 3A,B, Material and Methods). Surprisingly, our analyses revealed that the lateral amnion remained a ventral tissue until after the onset of germband retraction. The amnion cells essentially remained in the basolateral orientation that they presumably obtained when they separated from the serosa, and they neither reached the ventral midline nor closed a ventral epithelium (Figure 3B, supplementary Video 1, 2).

Coinciding with the onset of germband retraction, the amnion cells started to form filopodia-like protrusions that seemed to crawl toward the dorsal side of the embryo (Figure 3C,C’), possibly by using the serosa as substrate. As the amnion cells approached the lateral midline, they started flipping over such that their apical side came to lie against the basal side of the serosa and their basal side contacted the yolk sac (Figure 3C,C’). These cells then migrated from their ventrolateral position towards the dorsal midline. After germband retraction was completed, the amnion still remained open, but we started to observe extending and retracting filopodia-like protrusions of the amnion cells along the dorsal midline (Figure 3D,E).

To confirm our findings of an open rather than closed amnion, we used expression of a previously described marker for late amnion development, the tumor suppressor gene *Mab-eiger* (*Mab-egr*) (Kwan et al., 2016). We analyzed *Mab-egr* expression during germband

retraction, and found it expressed in a lateral narrow domain and in a posterior domain surrounding the dorsal opening; in some embryos we could observe stained protrusions similar to the filopodia-like structures seen in the time-lapse recordings. These results fully support our finding that the Megaselia amnion remains an open tissue until after germband retraction.

Taken together, our analyses of amnion morphogenesis in *M.abdita* suggest a gradual transition in its evolution from the ancestral ventral amnion: like in *T.castaneum*, we find the Megaselia amnion was set up as a ventral tissue. Accordingly, the Megaselia amnion could be explained by a gradual reduction of amnion size, which constrained amnion spreading and eventually resulted in a ventral open amnion.

The serosa forms a supracellular actin cable and spreads actively

To test whether gradual changes in serosa development could explain the evolutionary transition from intermediate to derived extraembryonic development as in *D.melanogaster*, we used *in toto* time-lapse recordings and visualized the dynamics of Megaselia serosa development. First signs of the serosa outline could be observed at around 60% GBE. At this time, Lifeact staining at the interface of amnion and serosa started to increase (Figure 4A,A'), suggesting the accumulation of F-actin and the formation of a supracellular actin cable at the serosa/amnion interface like in *T.castaneum* (Benton et al., 2013; Panfilio et al., 2013). In the following, actin accumulation persisted and increased at the serosa boundary (Figure 4B-C). As the serosa spread over the adjacent amnion, the actin cable followed as the amnion folded underneath the serosa (Figure 4D,D', supplementary Video 3, 4). Following this amniotic folding, the serosa continued to spread laterally and eventually broke free, leaving behind a single row of amnion cells. After disjunction of the two extraembryonic tissues, the actin cable was observed in the expanding serosa but not in the remaining amnion.

To quantify the dynamics of serosa spreading in *M.abdita*, we analyzed tissue expansion at the level of tissue area increase (Figure 5A-C, supplementary Video 5, 6) and at the level of individual serosa cell behavior (Figure 5D-E'). During germband extension, the serosa expanded at a constant rate of about 2.3 x 10^3 μm^2/min from about 15% of embryo coverage at mid germband extension to 30% coverage at the end of germband extension (Figure 5A,C). This first phase of serosa spreading was followed by a period of about 30 minutes, during which the expansion of the serosa seemed interrupted and did not increase substantially in area (Figure 5C).

While serosa expansion paused, we first observed changes in the behavior of serosa cells. Cells that were not in contact with the peripheral actin cable started to show increased changes in the apical area (Figure 5D-D'); similar pulsations were not observed in cells directly in contact with the actin cable (Figure 5E,E'). Following the changes in cell behavior, we could observe the separation of the serosa from the adjacent tissue towards the end of this intermission. This disjunction occurred directly after the increase of cell oscillations, and cell oscillations coincided with pulsations observed in the yolk. We therefore propose that the observed cell oscillations in the serosa were part of the process that decouples it from the yolk sac, with which the serosa is initially in tight contact (Schmidt-Ott and Kwan, 2016).

Consistent with a gradual detachment of the serosa from adjacent and underlying tissues, the serosa did not separate all at once but first at the anterior front, then at the posterior, and last at the lateral front (Figure 5B,C). Once the serosa was detached, it continued to expand over the embryo proper, and was completed during ventral closure, during which the two sides of the serosa fused at the ventral midline without apparent formation of filopodia (Figure 5F,G).

Notably the rate of tissue expansion was increased during the second phase of serosa spreading (Figure 5C). It was about three times higher than during the initial expansion, suggesting that, once the tissue broke free from the amnion, serosa cells actively contributed to tissue expansion, either through cell shape change, through active migration on the underlying tissue, or through crawling on the egg shell. Homogenous serosa spreading was observed at a rate of about 3.9 x 10^3 μm^2/min and appeared to be independent of the position of the actin cable (Figure 5A-A''',C), suggesting a strong contribution of cell flattening to serosa spreading. Similar changes in cell shapes have been described previously for the Drosophila amnioserosa (Pope and Harris, 2008).

Taken together, our analyses of serosa morphogenesis in *M.abdita* suggest that the Megaselia serosa shares cellular characters with the amnioserosa. In both tissues, cells expand dramatically and much more pronounced than seen for the Megaselia amnion (Figure 2J). However, we could not exclude that lack of cell flatting in the amnion resulted from tissue-level differences due to a much smaller area of the amnion compared to the serosa.

The serosa but not a dorsal amnion contributes to Drosophila-like germband retraction

To test whether the pulsatile cell behavior we observed in the serosa but not the amnion was dependent on tissue size, we wanted to analyze cell behavior in a larger amnion. Previous work had shown that knockdown of the homeodomain transcription factor Zerknüllt (Zen) in *M.abdita* transformed serosa into amnion cells and thus resulted in an enlarged amnion (Rafiqi et al., 2008). Accordingly, we analyzed tissue and cell behavior in SPIM time-lapse recordings after knockdown of Mab-zen and observed a dorsal amnion that did not show any evidence of epithelial expansion (Figure 6A-C). Quantification of extraembryonic cell behavior showed those cells to be amnion-typical and non-pulsatile (Figure 6D,D'). These results suggest that Megaselia amnion cell behavior was not dependent on tissue size, and rather specified by tissue fate and differentiation.

To test additional extraembryonic properties that could help to homologize the function of either Megaselia amnion or serosa with the amnioserosa in *D.melanogaster*, we asked whether either tissue contributed to embryonic morphogenesis similar to what has been reported previously in *D.melanogaster* (Lamka and Lipshitz, 1999; Schöck and Perrimon, 2003; Yip et al., 1997). To assess the function of extraembryonic tissues in germband morphogenesis, we used time- lapse recordings to quantify the dynamics of germband extension and retraction in *M.abdita*, and compared these dynamics between wildtype and *Mab-zen* RNAi embryos. Our results indicated that the initial phase of germband extension was not affected in *Mab-zen* RNAi embryos (Figure 6E). However, we found that the overall

degree of germband extension was notably reduced, and also retraction of the germband was affected in embryos lacking a serosa: it started earlier and was yet slower than in wildtype (Figure 6E), suggesting that cell and tissue properties of the spreading serosa were required for accelerated germband morphogenesis in *M.abdita*.

To test whether differences in germband dynamics of Megaselia embryos with either a serosa or a dorsal amnion could inform amnioserosa evolution, we asked whether evolution of the dorsal, non-spreading amnioserosa was associated with effects on extraembryonic cell behavior and germband morphogenesis comparable to *Mab-zen* RNAi embryos. To this end we analyzed the dynamics of germband extension and retraction in Drosophila embryos. As expected, we found that the amnioserosa lacked clear signs of tissue-level spreading (Figure 6F-H). However, rather than lacking cell oscillations like the amnion in *Mab-zen* RNAi embryos, cells in the amnioserosa exhibited pronounced oscillations similar to that seen in cells of the Megaselia serosa (Figure 6I,I', compare with Figure 5D,D'). Supporting the idea that the amnioserosa could have maintained serosa functionality, we found the dynamics of germband extension and retraction in *D.melanogaster* more reminiscent of Megaselia wildtype than of *Mab-zen* RNAi embryos (Figure 6J).

Taken together, our results indicate that differences exist between a genetically and evolutionary generated non-spreading extraembryonic epithelium. Rather than being exclusively derived from a dorsal amnion, our analyses suggest that the late amnioserosa retained at least some serosa properties and originated without a disruptive transformation of serosa development.

Yolk expression of ECM remodeling enzyme contributes to timing and onset of serosa spreading

In search for alternative mechanisms that affected epithelial spreading without changing fate and differentiation of extraembryonic tissues, we reasoned that extraembryonic tissue dynamics may be sensitive to the remodeling of extracellular adhesion between serosa and underlying membranes. A candidate gene that is known for its ability to remodel extracellular adhesion in various contexts is the *matrix metalloprotease 1* (*mmp1*). In *D.melanogaster*, *mmp1* has been linked to the remodeling of basal-basal tissue contacts, e.g. during folding in wing disc formation (Sui et al., 2012) and head eversion (Page-McCaw et al., 2003). During early Drosophila embryonic development, however, *mmp1* is only weakly expressed and no phenotype has been observed in embryos mutant for *mmp1* (Page-McCaw et al., 2003).

In *M.abdita*, we found *Mab-mmp1* expressed within the yolk sac (Figure 7A), which provides a third but often neglected extraembryonic membrane (Schmidt-Ott and Kwan, 2016). To assess its function, we used *Mab-ddc* as serosa marker gene (Rafiqi et al., 2010) and compared wildtype embryos with embryos in which *Mab-mmp1* activity had been reduced by RNAi or by mosaic loss-of-function using embryonic CRISPR/Cas9 (Figure 7B-D). We found that the serosa did not detach in time in *Mab-mmp1* RNAi (n=100/104) and *Mab-mmp1* CRISPR embryos (n=77/136), and instead appeared to be dragged towards the anterior pole in a manner reminiscent of amnioserosa tissue morphology in Drosophila embryos.

To assess how cell and tissue dynamics were affected in embryos with reduced *Mab-mmp1* activity, we performed time-lapse recordings of *Mab-mmp1* RNAi embryos (Figure 7E-G).

Pulsation and oscillation in *Mab-mmp1* RNAi embryos were present but dampened (Figure 7H,H') and continued for about double the time as in wildtype. Specifically, cells seemed to be "stuck" after their first, initial contraction, and only later loosened to a degree similar to the wildtype. Coinciding with contracting serosa cells getting stuck to the underlying yolk sac, we observed a substantial amount of "dragging" towards the anterior pole, leading to an outline of the serosa similar to that of *Mab-ddc* staining in fixed *Mab-mmp1* RNAi embryos (Figure 7C). While we found reduced activity of *Mab-mmp1* to be sufficient to change the dynamics of the extraembryonic tissues behavior and substantially delay the disjunction of serosa and amnion, knockdown of *Mab-mmp1* by RNAi and mosaic knockout by CRISPR did not affect the embryonic development; treated embryos showed the same germband extension and retraction dynamics of Megaselia wild type embryos (Figure 7I).

Taken together, our results suggest that the Megaselia yolk sac contributes to overall extraembryonic morphogenesis, which confirms previous predictions (Anderson, 1972a; Benton et al., 2013; Handel et al., 2000; Schmidt-Ott and Kwan, 2016). Functional interference with the coupling of serosa and yolk sac revealed a powerful mechanism to change the spreading behavior of the serosa. The developing serosa in *Mab-mmp1* RNAi embryos passes through stages that are phenotypically very similar to the amnioserosa in *D.melanogaster*, indicating that such a mechanism could have played a role in a gradual evolution of the amnioserosa as a single dorsal extraembryonic epithelium.

DISCUSSION

Our analysis of amnion and serosa development in the scuttle fly *Megaselia abdita* has allowed us to identify cellular, epithelial, and functional properties for the two distinct extraembryonic tissues. In the serosa, cells in apposition to the yolk sac show oscillation, the epithelium spreads tissue-autonomously at a rate comparable to, e.g., expansion of the outer enveloping layer during zebrafish epiboly (2.8 to 3.1 x 10^3 μm^2/min, see material and methods), and in its function the serosa aids morphogenetic movements of the embryo germband during late developmental stages. Similar epithelial properties have been observed previously in the beetle *Tribolium castaneum* (Benton, 2013; Benton et al., 2013; Hilbrant et al., 2016; Panfilio et al., 2013), suggesting that the features described here for the first time in *M.abdita* represent conserved characters of the insect serosa. In the amnion, we could not find evidence of cell oscillation and tissue spreading, even when its tissue size was substantially enlarged. Notably, we found that the single dorsal amnion developing in *Mab-zen* RNAi embryos could not substitute for the serosa in aiding late embryo morphogenesis.

Our results indicate that *M.abdita* develops a ventral amnion. This amnion shares properties with the ventral amnion in *T.castaneum*. In contrast to the Tribolium amnion, the Megaselia amnion did not fuse along the ventral midline but remained open. On the one hand, lack of ventral amnion closure in *M.abdita* could be explained by differences in amnion size. Accordingly, a larger amnion in *T.castaneum* could allow for more extensive tissue expansion and thus the closure of the ventral amnion. However, recent observations suggests that the Tribolium amnion may not be as large as previously assumed (Benton, 2017), and also mosquitoes and midges, which form a complete ventral amnion, do not seem

to feature a substantially larger amnion anlage than *M.abdita*. On the other hand, then, differences in complete versus incomplete ventral closure could stem from differences in germband properties. Recent work in *T.castaneum* suggests that part of the germband can fold over and underneath the embryo, thus resulting in a rather narrow gap that needs to be covered by the amnion (Benton, 2017). Likewise, the germband compacts very tightly in mosquitoes and midges, which leaves a similarly narrow gap to be closed by the ventral amnion. The overall similarities between Megaselia and Tribolium amnion in topology, properties, and previously described genetics suggest, however, that the program of amnion cell and tissue development and differentiation are essentially conserved. We therefore propose that the evolution of the ventrally open Megaselia amnion from a Tribolium-like ancestor occurred by a gradual and continuous transition, either through stepwise reduction of amnion size or an increasing width and stiffness in the developing germband.

Our analysis of serosa properties and function in *M.abdita* revealed features of serosal heritage that we also found present in the Drosophila amnioserosa. These results are at odds with the obvious topological differences in the setup of extraembryonic epithelia in Drosophila and most other insects, and we cannot exclude the possibility that the amnioserosa evolved its serosa-like properties independently. However, we consider it more likely that cellular and functional similarity of serosa and amnioserosa reflect common descent and are evidence for evolution of a developmental novelty by gradual change. Specifically, we propose that the amnioserosa originated by a gradual loss of serosa spreading. We could demonstrate that a gradual reduction of Megaselia serosa spreading did not disrupt its epithelial integrity but only delayed serosa expansion. These results illustrate how loss of tissue spreading could evolve as a gradual process in which intermediate stages remained viable. The complete transition from a spreading to a non-spreading extraembryonic tissue most likely involved more than one gene regulating the interaction between different extraembryonic membranes. This gradual transition does not need to invoke remodeling in extraembryonic development and cell differentiation, and we argue that major elements of amnion and serosa development were still present in the ‘ur-amnioserosa’. This implies that the amnioserosa, at least initially, constituted a composite extraembryonic epithelium made up of amnion as well as serosa. Sharply defined distinctions between amnion and serosa may be lost in today’s amnioserosa, but support for differently behaving areas in the amnioserosa has been pointed out before, such as distinct cell behavior in terminal and central domains and diverging promotor activities between central and peripheral cells (Gorfinkiel et al., 2009; Wada et al., 2007).

The striking differences in extraembryonic architecture of insects provide a unique paradigm to test how morphogenetic novelty can arise in spite of deeply conserved developmental programs. We have shown how morphogenetic novelty can result from gradual changes in the interaction between distinct tissues. Because these changes presumably leave the core of developmental regulation unaffected, they may represent a more general mechanism that allowed the evolution of morphogenetic novelty regardless of deep conservation in patterning and cell differentiation.

MATERIAL AND METHODS

Fly stocks

The laboratory culture of Megaselia abdita (Sander strain) was maintained at 25℃ and a constant 16/8-hr day/night cycle as described previously (Caroti et al., 2015). *sqh-Gap43::mCherry/CyO* (gift from Stefano De Renzis) was used to label membranes in Drosophila melanogaster recordings.

Cloning and RNA synthesis

Mab-mmp1 was identified from genome and transcriptome sequences. A genomic fragment (GenBankID01) was cloned after PCR amplification from the locus, a cDNA fragment after amplification through 5'-RACE (GenBankID02). Double-stranded RNA (dsRNA) was synthesized as described (Urbansky et al., 2016); *Mab-mmp1* dsRNA comprised pos. +103 to +1167 of the genomic fragment (pos. 1 refers to first nucleotide in ORF) and included a 57bp intron at pos. +575; *Mab-zen* dsRNA was based on a previously published fragment (Stauber et al., 2002). Guide RNAs for a knock-out of *Mab-mmp1* were designed using CCTop as CRISPR/Cas9 target online predictor (Stemmer et al., 2015). Three single guide RNAs (sgRNAs) were designed to target the following positions (pos. 1 refers to first nucleotide in ORF): sgRNA1, 5'-TGCAGAGCGTATCTCTTT, pos +404 to +387; sgRNA2, 5'-CGTGGACTATTGATTGTC, pos +710 to +693; sgRNA3, 5'-TCGGCAACCGAGTTTTCA, +898 to +881. Guide RNAs as well as Cas9 mRNA were synthesized as described (Stemmer et al., 2015).

Preparation of Lifeact-eGFP, Lifeact-mCherry, and Histone H1

Heterologous expression vectors for Lifeact-eGFP and Lifeact-mCherry were generated by cloning PCR-amplified Lifeact-FP fusion constructs into pET-21a(+). Lifeact-eGFP was amplified from pT7-LifeAct-EGFP (Benton et al., 2013) using primer pair 5'-AAACATATGGGCGTGGCCGATCTGAT/5'-TTTTCTCGAGCTTGTACAGCTCGTCCATGC, digested with *Nde*I and *Xho*I, and cloned into pET-21a(+) to generate pET-Lifeact-eGFP. Similarly, mCherry was amplified from H2Av-mCherry (Krzic et al., 2012) using primer pair 5'-GAGGGGATCCTCGCCACCAGATCCATGGTGAGCAAGGGCGAGGAG/5'-GGTGCTCGAGGGCGCCGGTGGAGTGGCGGCC, digested with *Bam*HI and *Xho*I, and replaced eGFP in pET-Lifeact-eGFP with mCherry to generate pET-Lifeact-mCherry.

Recombinant Lifeact-FP protein was expressed in *E.coli* BL21 after induction with IPTG (final concentration 1mM) at OD_{600}=0.6-0.8. Cells were pelleted 4 hrs after induction, washed in PBS, and resuspended in lysis buffer on ice (50 mM NaPO4 pH 8.0, 0.5 M NaCl, 0.5% glycerol, 0.5% Tween-20, 10 mM imidazole, 1 mg/ml lysozyme). Resuspended cells were sonicated with 15-30 s pulses, centrifuged, and the supernatant mixed with equilibrated Ni-NTA agarose beads (Cube Biotech, Germany). Protein binding was carried out for 2 hrs at 4°C, beads were washed three times at high-salt/high-pH (50 mM NaPO4 pH 8.0, 250 mM NaCl, 0.05% Tween-20, 20 mM imidazole), once at high-salt/low-pH (50 mM NaPO4 pH 6.0, 250 mM NaCl, 0.05% Tween-20, 20 mM imidazole), and twice at high-salt/high-pH without detergent (50 mM NaPO4 pH 8.0, 250 mM NaCl, 20 mM imidazole). Following the washes, beads were transferred into a poly-prep chromatography column (BioRad Laboratories) and the protein was eluted in multiple aliquots of elution buffer (50 mM NaPO4 pH 8.0, 150 mM NaCl, 250 mM imidazole, 5% glycerol). Collected protein fractions were analyzed by SDS-PAGE and dialyzed against PBS. Final concentrations were typically around 0.5 mg/ml; aliquots were stored at -80°C.

Histone H1 (Merck/Calbiochem) was fluorescently tagged using Texas Red™-X Protein Labeling Kit (ThermoFisher) as described (Mori et al., 2011). Final concentration was typically around 2 mg/ml; 10% saturated sucrose was added as anti-frost reagent, and aliquots were stored at -80°C.

Immunohistochemistry

For whole mount *in situ* hybridization using NBT/BCIP as stain, embryos were heat fixed, devitellinized using a 1+1 mix of n-heptane and methanol, and post-fixed using 5% formaldehyde as described (Rafiqi et al., 2011a). For *in situ* hybridization using fluorescent Fast Red (Sigma-Aldrich), embryos were fixed with 4% formaldehyde and devitellinized using a 1+1 mix of n-heptane and methanol. For staining with phallacidin and DAPI, embryos were fixed with 4% formaldehyde and devitellinized using a 1+1 mix of n-heptane and 90% ethanol (Mathew et al., 2011). Whenever necessary, manual devitellinization was performed as described (Rafiqi et al., 2011a).

RNA probe synthesis, whole mount in situ hybridization, and detection was carried out as described (Lemke and Schmidt-Ott, 2009). The following cDNA fragments were used as probes: Mab-ddc (Rafiqi et al., 2010), Mab-egr (Kwan et al., 2016), and Mab-zen (Stauber et al., 1999), and the newly cloned *Mab-mmp1* cDNA fragment. Phallacidin staining was performed as described (Panfilio and Roth, 2010) with modifications: the stock (200 units/ml, Invitrogen B607) was diluted in PBS (1:25), embryos were stained for 3 hrs at room temperature and then briefly rinsed three times in PBS. DNA was stained using 4',6-diamidino-2-phenylindole (DAPI, Life Technology D1306) at a final concentration of 0.2 µg/ml.

Injections

Embryos were collected, prepared for injection, and injected essentially as described (Rafiqi et al., 2011b). dsRNA was injected with concentrations of 1 mg/ml (*Mab-zen*) and 3.9 mg/ml (*Mab-mmp1*), which corresponded to about 2 µM of *Mab-zen* and 6 µM of Mab-mmp1 dsRNA. Concentration of injected Lifeact-mCherry protein was about 0.5 mg/ml, Histone H1 was injected at concentrations of about 0.7 mg/ml. Cas9 mRNA and all three sgRNAs were co-injected as a mix with a final concentration of 1 mg/ml of Cas9 mRNA and 50 ng/ml for each of the sgRNAs (Bassett et al., 2013).

Microscopy

Embryos were embedded in a 3+1 mix of glycerol and PBS. Histochemical staining was recorded with DIC on a Zeiss Axio Imager M1 using 10x (dry, 10x/0.45); fluorescent staining was recorded by single-photon confocal imaging on a Leica system (SP8) using a 20x immersol objective (HC PL APO CS2 20x/0.75). Image stacks were acquired with a voxel size of 0.57 x 0.57 x 0.57 µm by oversampling in z.

Light-sheet microscope setup and imaging

Time-lapse recordings were performed using two Multiview light-sheet microscopes (MuVi-SPIM) (Krzic et al., 2012) with confocal line detection (de Medeiros et al., 2015). The microscopes were equipped with two 25 × 1.1 NA water immersion objective lenses (CFI75 Apo LWD 25XW, Nikon) or two 16 × 0.8 NA water immersion objective lenses (CFI75 Achro LWD 16XW, Nikon) for detection. Illumination was performed via two 10 × 0.3 NA water immersion objective lenses (CFI Plan Fluor 10XW). All objectives were used with the

corresponding 200 mm tube lenses from Nikon. Fluorescence of mCherry was excited at 561 nm or 594 nm, TexasRed at 642 nm. Fluorescence was imaged simultaneously onto two sCMOS cameras (Hamamatsu Flash 4 V2) after passing corresponding fluorescence filters on the detection paths (561 nm LP, 647 nm LP, 594 nm LP, EdgeBasic product line, Semrock).

M.abdita embryos were injected in oil (refractive index 1.335, Cargille Labs) and mounted in an oil-filled fluorinate ethylene propylene (FEP) tube (Kaufmann et al., 2012). This tube was stabilized with a glass capillary that was placed into the capillary holder of the microscope. Transgenic *D.melanogaster* embryos were mounted in gel as described (Krzic et al., 2012). All embryos were imaged from 4 sides (one 90° rotation) every 1.5 or 2 min with a z-spacing of 1 µm for membrane labeled embryos and 2 µm for nuclear labeled embryos. The four orthogonal views facilitated a more uniform sampling, and the typical exposure time per plane of around 40 ms guaranteed an overall high temporal resolution. The resultant 4 stacks per time point were fused using previously published software (Krzic et al., 2012; Preibisch et al., 2010). All further processing and analysis was performed on the fused data sets. Analysis of embryonic development was based on a total of 12 MuVi-SPIM recordings, i.e. *M.abdita* wildtype (n=3), *D.melanogaster* wildtype (n=2), *M.abdita* zen RNAi (n=4), and *M.abdita* mmp1 RNAi (n=3) (see complete list of movies in Figure 2 – figure supplement 1). To register embryonic development within and between species, the dynamics of the initial, fast phase of germband extension were used as reference (Rauzi et al., 2015).

Generation of embryo point clouds at and below the surface level

To allow for rapid image operations, fused 3D image stacks of individual MuVi-SPIM time points were transformed into point clouds. Time-adaptive intensity thresholding was used to segment the 3D image stacks into exactly two solid components: embryo and background. If segmentation returned more than one object, all but the largest one were eliminated and holes resulting from a lower fluorescence intensity in the yolk area were filled. To reveal fluorescent signal in layers below the embryo surface, the outermost layer of the segmented embryo was eroded using morphological operators and a kernel radius of the specified depth. When needed, the surface was smoothened through morphological closing or opening. To visualize fluorescent signal for a specific layer of the embryo, the embryo was eroded at different depths and the resulting images subtracted from the original producing a set of concentric layers. Point clouds were generated by mapping the geometrical voxel information (width, height, and depth) into vectors representing the three-dimensional cartesian coordinates [X,Y,Z], and their respective intensities into an additional vector.

Projections

To quantify tissue spreading over the full surface of the fly embryo, we used cylindrical projections as described (Krzic et al., 2012; Rauzi et al., 2015). Briefly, the anterior-to-posterior axis of the egg was aligned along the Z axis of the cartesian coordinate system. Point cloud coordinates were then transformed into cylindrical coordinates [X,Y,Z]->[θ,r,Z]. For each position along Z and from 0 to 2π along θ, the mean intensities of all points between r_{max} and r_{min} were projected as pixels along width and height [W,H] of a two-dimensional image I. To allow for a mapping of information obtained in I (tissue areas and cell tracks) back to the point clouds and stacks, the index information of all projected points was kept in a vector array. Our cylindrical projection provided an approximate area conservation in the central domain of the embryo that was sufficient for visualization purposes. For quantitative analyses of serosa expansion, distortions were corrected at poles

and furrows by using the law of cosines to weight the area of each pixel in I according to its contribution to the corresponding surface voxel in the embryo.

Membrane segmentation

To quantify main aspects of cell shapes in fixed tissue, phallacidin stained cells were segmented semi-automatically using Ilastik (Linux version 1.2.0) Pixel Classification framework (Sommer et al., 2011); challenging domains were fully trained within iLastik. Predictions were exported as a binary image stack. The spatial position of each cell within the imaged volume was defined by the centroid of the segmented cell. Individual cell volumes were extracted as a single connected component, the resulting objects were loaded as point clouds into Matlab and remaining holes were closed using fillholes3d (maximal gap 20px). To account for possible artifacts in image processing, objects smaller than 200 px and larger than 10000 px were excluded from further analyses. To reveal changes in cell and tissue dynamics in time-lapse recordings, individual cells and the expanding serosa were outlined manually.

Speed of tissue closure

To quantify the zippering rates of ventral serosa closure (*M.abdita*) and dorsal amnioserosa closure (*D.melanogaster*), height and width of the tissue openings were followed over time. Fitted constants, V (relative velocity of the leading edge) and kz (the rate constant of zipping), were obtained using the published model of D.melanogaster dorsal closure (Hutson et al., 2003).

Feature extraction and quantification

Cell height was measured as object length orthogonal to the embryo surface. Cell surface area and cell circularity were measured by a 2D footprint that was obtained through a projection of the segmented cell body along the normal axis of the embryo. Cell tracks were obtained manually by following cells in selected layers of cylindrical projections. Cell pulsation was measured as change of apical area in consecutive time points using manual markings on cylindrical projections of the embryo. Germband extension was measured in mid-sagittal sections of time-lapse recordings: the most anterior point of the dorsally extending germband was used as reference, and germband extension was measured in percent egg length relative to the anterior-posterior length of the embryo. Ventral closing of the serosa was quantified by measuring height and width of the serosal window over time. The relative velocity of the leading edge (V) and the rate constant of serosa zipping (kz) were obtained using the rate-process model of dorsal closure in *D.melanogaster* (Hutson et al., 2003).

Rates for tissue expansion were calculated for M.abdita serosa and zebrafish enveloping layer (EVL) based on relative tissue expansion and embryo or tissue surface area. In *M.abdita*, the serosa increased in size by about 1.5% of the total embryo area per minute during free tissue expansion (Figure 4D). The outer embryo surface area was measured at the blastoderm stage with 3.8×10^6 pixel area units, pixel area was 0.26 x 0.26 μm^2, and overall expansion rate thus 3.9×10^3 μm^2/min. In zebrafish, EVL area increased in size by about 0.18% of the total embryo area per minute during 35% to 100% epiboly (Keller et al., 2008). The outer embryo surface area was approximated as sphere with a diameter of 700 µm (Kimmel et al., 1995), resulting in an overall expansion rate of 2.8×10^3 μm^2/min. A similar rate for EVL expansion was obtained based on measures of EVL cell area expansion by about 0.40% in the first hundred minutes after 55% epiboly (Campinho et al., 2013). At 55% epiboly, the EVL is comprised of about 1080 cells with a mean apical cell area of 710

μm^2 (Campinho et al., 2013), resulting in an overall tissue expansion rate of 3.1 x 10^3 μm^2/min. Differences between the two estimates of EVL expansion may stem from measurement uncertainties or reflect different dynamics due to cell divisions in early EVL expansion, which become negligible after 55% epiboly stage (Campinho et al., 2013).

Principal component analysis

The principal component analysis comprised three developmental stages (cellular blastoderm, germband extension, serosa spreading), and cells were each described by their height, area, and area circularity. All parameters were normalized by z-score normalization. Based only on parameter values and covariance, the analysis identified the two main axes along which variation in our data set was maximal. For all sections, the resulting two principal components (PC1 and PC2) accounted for 77% and 16% of variance, respectively. A biplot for the PCA was generated to visualize the contribution of each of the parameters to the two principal components. To test whether parameter separation was dependent on developmental age and cell differentiation, we binned and color-coded cells according to the two main clusters, mapped them back onto raw images, and visually determined whether they belonged to embryonic or extraembryonic tissue.

General image processing

3D reconstruction images of individual cells from z-stack segmentation data were done in Matlab (R2016b), images and stacks were processed using Fiji (2.0.0-rc-34/1.50a) and Matlab, and panels were assembled into figures in Adobe Photoshop and Adobe Illustrator.

ACKNOWLEDGEMENTS

We thank A Guse and N Bloch for help with establishing a protocol for recombinant Lifeact-GFP; P Lenart for suggesting the use of labeled H1; M Benton, L Centanin, N Gorfinkiel, A Guse, K Panfilio, U Schmidt-Ott, J Wittbrodt, and members of the Lemke lab for discussions and/or comments on the manuscript; I Lohmann, J Lohmann and J Wittbrodt for sharing laboratory equipment; and A Maizel and J Wittbrodt for generous support. Funded by DFG grant LE 2787/1-1, HFSP grant RGY0082/2015, and a pre-doctoral HBIGS fellowship to LS.

AUTHOR CONTRIBUTIONS

FC, Conception and design, acquisition of data, analysis and interpretation of data, drafting or revising manuscript; EGA, Processing, analysis and interpretation of data; PGA, Analysis and interpretation of data, drafting or revising manuscript; VN, Acquisition of data, analysis and interpretation of data, drafting or revising manuscript; DK, Acquisition of data, analysis and interpretation of data; LS, Processing of data and contributed essential computational infrastructure; MW, contributed essential unpublished reagents; LH, Analysis and interpretation of data; SL, Conception and design, analysis and interpretation of data, drafting and writing manuscript.

COMPETING INTERESTS

The authors declare no competing interests.

REFERENCES

Anderson, D. T. (1972a). The development of holometabolous insects. In *Developmental Systems: Insects* (eds. Counce, S. and Waddington, C., pp. 165–242. Academic Press (London/New York).

Anderson, D. T. (1972b). The development of hemimetabolous insects. In *Developmental Systems: Insects* (eds. Counce, S. J. and Waddington, C., pp. 95–163. Academic Press (London/New York).

Bassett, A. R., Tibbit, C., Ponting, C. P. and Liu, J.-L. (2013). Highly Efficient Targeted Mutagenesis of Drosophila with the CRISPR/Cas9 System. *Cell Rep* **4**, 220–228.

Benton, M. A. (2013). Analysis of embryonic development in Tribolium castaneum using a versatile live fluorescent labelling technique. PhD thesis.

Benton, M. A. (2017). A revised understanding of Tribolium morphogenesis further reconciles short and long germ development. *bioRxiv*. doi.org/10.1101/232751

Benton, M. A., Akam, M. and Pavlopoulos, A. (2013). Cell and tissue dynamics during Tribolium embryogenesis revealed by versatile fluorescence labeling approaches. *Development* **140**, 3210–3220.

Campinho, P., Behrndt, M., Ranft, J., Risler, T., Minc, N. and Heisenberg, C.-P. (2013). Tension-oriented cell divisions limit anisotropic tissue tension in epithelial spreading during zebrafish epiboly. *Nat Cell Biol* **15**, 1405–1414.

Campos-Ortega, J. A. and Hartenstein, V. (1997). *The Embryonic Development of Drosophila Melanogaster*. Springer, Berlin, Heidelberg, New York.

Caroti, F., Urbansky, S., Wosch, M. and Lemke, S. (2015). Germ line transformation and in vivo labeling of nuclei in Diptera: report on Megaselia abdita (Phoridae) and Chironomus riparius (Chironomidae). *Development Genes and Evolution* **225**, 179–186.

Darwin, C. (1872). *The Origin of Species*. 6 ed. London: John Murray.

de Medeiros, G., Norlin, N., Gunther, S., Albert, M., Panavaite, L., Fiuza, U.-M., Peri, F., Hiiragi, T., Krzic, U. and Hufnagel, L. (2015). Confocal multiview light-sheet microscopy. *Nat Commun* **6**, 8881.

Gorfinkiel, N., Blanchard, G. B., Adams, R. J. and Martinez Arias, A. (2009). Mechanical control of global cell behaviour during dorsal closure in Drosophila. *Development* **136**, 1889–1898.

Hallgrímsson, B., Jamniczky, H. A., Young, N. M., Rolian, C., Schmidt-Ott, U. and Marcucio, R. S. (2012). The generation of variation and the developmental basis for evolutionary novelty. *J Exp Zool B Mol Dev Evol* **318**, 501–517.

Handel, K., Grünfelder, C. G., Roth, S. and Sander, K. (2000). Tribolium embryogenesis: a SEM study of cell shapes and movements from blastoderm to serosal closure. *Development Genes and Evolution* **210**, 167–179.

Hilbrant, M., Horn, T., Koelzer, S. and Panfilio, K. A. (2016). The beetle amnion and serosa functionally interact as apposed epithelia. *Elife (Cambridge)* **5**.

Horn, T., Hilbrant, M. and Panfilio, K. A. (2015). Evolution of epithelial morphogenesis: phenotypic integration across multiple levels of biological organization. *Front Genet* **6**,

303.

Hutson, M. S., Tokutake, Y., Chang, M.-S., Bloor, J. W., Venakides, S., Kiehart, D. P. and Edwards, G. S. (2003). Forces for morphogenesis investigated with laser microsurgery and quantitative modeling. *Science* **300**, 145–149.

Kaufmann, A., Mickoleit, M., Weber, M. and Huisken, J. (2012). Multilayer mounting enables long-term imaging of zebrafish development in a light sheet microscope. *Development* **139**, 3242–3247.

Keller, P. J., Schmidt, A. D., Wittbrodt, J. and Stelzer, E. H. K. (2008). Reconstruction of zebrafish early embryonic development by scanned light sheet microscopy. *Science* **322**, 1065–1069.

Kimmel, C. B., Ballard, W. W., Kimmel, S. R., Ullmann, B. and Schilling, T. F. (1995). Stages of embryonic development of the zebrafish. *Dev Dyn* **203**, 253–310.

Krzic, U., Gunther, S., Saunders, T. E., Streichan, S. J. and Hufnagel, L. (2012). Multiview light-sheet microscope for rapid in toto imaging. *Nat Methods* **9**, 730–733.

Kwan, C. W., Gavin-Smyth, J., Ferguson, E. L. and Schmidt-Ott, U. (2016). Functional evolution of a morphogenetic gradient. *Elife (Cambridge)* **5**.

Lamka, M. L. and Lipshitz, H. D. (1999). Role of the amnioserosa in germ band retraction of the Drosophila melanogaster embryo. *Dev Biol* **214**, 102–112.

Lemke, S. and Schmidt-Ott, U. (2009). Evidence for a composite anterior determinant in the hover fly Episyrphus balteatus (Syrphidae), a cyclorrhaphan fly with an anterodorsal serosa anlage. *Development* **136**, 117–127.

Mori, M., Monnier, N., Daigle, N., Bathe, M., Ellenberg, J. and Lénárt, P. (2011). Intracellular transport by an anchored homogeneously contracting F-actin meshwork. *Curr Biol* **21**, 606–611.

Page-McCaw, A., Serano, J., Santé, J. M. and Rubin, G. M. (2003). Drosophila matrix metalloproteinases are required for tissue remodeling, but not embryonic development. *Dev Cell* **4**, 95–106.

Panfilio, K. A. and Roth, S. (2010). Epithelial reorganization events during late extraembryonic development in a hemimetabolous insect. *Dev Biol* **340**, 100–115.

Panfilio, K. A., Oberhofer, G. and Roth, S. (2013). High plasticity in epithelial morphogenesis during insect dorsal closure. *Biol Open* **2**, 1108–1118.

Pope, K. L. and Harris, T. J. C. (2008). Control of cell flattening and junctional remodeling during squamous epithelial morphogenesis in Drosophila. *Development* **135**, 2227–2238.

Preibisch, S., Saalfeld, S., Schindelin, J. and Tomancak, P. (2010). Software for bead-based registration of selective plane illumination microscopy data. *Nat Methods* **7**, 418–419.

Rafiqi, A. M., Lemke, S. and Schmidt-Ott, U. (2010). Postgastrular zen expression is required to develop distinct amniotic and serosal epithelia in the scuttle fly Megaselia. *Dev Biol* **341**, 282–290.

Rafiqi, A. M., Lemke, S. and Schmidt-Ott, U. (2011a). Megaselia abdita: fixing and devitellinizing embryos. *Cold Spring Harb Protoc* **2011**, pdb.prot5602.

Rafiqi, A. M., Lemke, S. and Schmidt-Ott, U. (2011b). Megaselia abdita: preparing embryos for injection. *Cold Spring Harb Protoc* **2011**, pdb.prot5601.

Rafiqi, A. M., Lemke, S., Ferguson, S., Stauber, M. and Schmidt-Ott, U. (2008). Evolutionary origin of the amnioserosa in cyclorrhaphan flies correlates with spatial and temporal expression changes of zen. *Proc Natl Acad Sci USA* **105**, 234–239.

Rafiqi, A. M., Park, C.-H., Kwan, C. W., Lemke, S. and Schmidt-Ott, U. (2012). BMP-dependent serosa and amnion specification in the scuttle fly Megaselia abdita. *Development* **139**, 3373–3382.

Rauzi, M., Krzic, U., Saunders, T. E., Krajnc, M., Ziherl, P., Hufnagel, L. and Leptin, M. (2015). Embryo-scale tissue mechanics during Drosophila gastrulation movements. *Nat Commun* **6**, 8677.

Schmidt-Ott, U. and Kwan, C. W. (2016). Morphogenetic functions of extraembryonic membranes in insects. *Curr Opin Insect Sci* **13**, 86–92.

Schöck, F. and Perrimon, N. (2003). Retraction of the Drosophila germ band requires cell-matrix interaction. *Genes Dev* **17**, 597–602.

Shubin, N. H., Daeschler, E. B. and Jenkins, F. A. (2006). The pectoral fin of Tiktaalik roseae and the origin of the tetrapod limb. *Nature* **440**, 764–771.

Sommer, C., Straehle, C., Kothe, U. and Hamprecht, F. A. (2011). Ilastik: Interactive learning and segmentation toolkit.pp. 230–233. IEEE.

Stauber, M., Jäckle, H. and Schmidt-Ott, U. (1999). The anterior determinant bicoid of Drosophila is a derived Hox class 3 gene. *Proc Natl Acad Sci USA* **96**, 3786–3789.

Stauber, M., Prell, A. and Schmidt-Ott, U. (2002). A single Hox3 gene with composite bicoid and zerknullt expression characteristics in non-Cyclorrhaphan flies. *Proc Natl Acad Sci USA* **99**, 274–279.

Stemmer, M., Thumberger, T., Del Sol Keyer, M., Wittbrodt, J. and Mateo, J. L. (2015). CCTop: An Intuitive, Flexible and Reliable CRISPR/Cas9 Target Prediction Tool. *PLoS ONE* **10**, e0124633.

Sui, L., Pflugfelder, G. O. and Shen, J. (2012). The Dorsocross T-box transcription factors promote tissue morphogenesis in the Drosophila wing imaginal disc. *Development* **139**, 2773–2782.

Urbansky, S., González Avalos, P., Wosch, M. and Lemke, S. (2016). Folded gastrulation and T48 drive the evolution of coordinated mesoderm internalization in flies. *Elife (Cambridge)* **5**.

van der Zee, M., Berns, N. and Roth, S. (2005). Distinct Functions of the Tribolium zerknu¨llt Genes in Serosa Specification and Dorsal Closure. *Current Biology* **15**, 624–636.

van der Zee, M., Stockhammer, O., Levetzow, von, C., Nunes da Fonseca, R. and Roth, S. (2006). Sog/Chordin is required for ventral-to-dorsal Dpp/BMP transport and head formation in a short germ insect. *Proc Natl Acad Sci USA* **103**, 16307–16312.

Wada, A., Kato, K., Uwo, M. F., Yonemura, S. and Hayashi, S. (2007). Specialized extraembryonic cells connect embryonic and extraembryonic epidermis in response to Dpp during dorsal closure in Drosophila. *Dev Biol* **301**, 340–349.

Xu, X., You, H., Du, K. and Han, F. (2011). An Archaeopteryx-like theropod from China and the origin of Avialae. *Nature* **475**, 465–470.

Yip, M. L., Lamka, M. L. and Lipshitz, H. D. (1997). Control of germ-band retraction in Drosophila by the zinc-finger protein HINDSIGHT. *Development* **124**, 2129–2141.

FIGURE LEGENDS

Figure 1. Quantitative analyses of cell measures reveal distinctive properties of embryonic and extraembryonic epithelia in *M.abdita* embryos at subsequent stages of development. (**A-Cb'**) Global embryonic view of fixed embryos stained for phallacidin to outline the actin cytoskeleton at subsequent stages of development (**A-C**), with close-up views (**Aa-Cb**) and three dimensional volume renderings (**Aa'-Cb'**) of embryonic (**Aa-a'**, **Ba-a'**, **Ca-a'**) and extraembryonic cells (**Ab-b'**, **Bb-b'**, **Cb-b'**). (**D-D''**) Biplots of a principal component analysis for cells of all *M.abdita* embryos analyzed; the first two principal components account for 93% of the overall observed variance. Shown is the distribution of all cells according to developmental stage (**D**), the contribution of features to the two first principal components (**D'**), and the clustering of cells into either embryonic or extraembryonic cells after evaluation of cell fate (**D''**, see methods). (**E-G**) Collective quantitative analysis of apical cell area (**E**), apical cell circularity (**F**) and relative cell height (**G**). Embryos and close-ups (**A-Cb**) are shown with anterior left. Cells (**Aa-Cb'**, **D'-G**) with shapes classified as blastodermal or embryonic are labeled green, cells classified as extraembryonic are labeled in dark grey. Scale bars, 10 µm.

Figure 2. Tracking of lateral cell dynamics distinguishes between two populations of extraembryonic cells and characterizes serosal and amniotic tissue spreading. (**A-E**) Global embryonic view of a time-lapse recorded embryo during germband extension (**A**) with a close-up view of expanding extraembryonic tissue (**B**). Based on their subsequent spreading over underlying cells at a later time point (**C**, **C'**), cells of the serosa (blue) could be distinguished from adjacent cells (orange) and then tracked back to the dorsal blastoderm (**D**). Based on cells tracked on either side of the embryo, the serosa anlage occupied a domain of six to seven cells centered on the dorsal midline, which perfectly coincided with the gene expression domain of the homeodomain transcription factor *zen* in fixed embryos (**E**). (**F-I**) Lateral cells about two to three rows adjacent to the serosa showed substantial increase of apical cell area compared to ectodermal cells. Cells directly adjacent to the serosa never divided and could be tracked back to a single cell row next to the serosa anlage (orange in **F-I**). More distal cells divided and eventually decreased in cell size (green in **F-I**). (**J**) Quantitative analysis of cell size of tracked serosa, amnion, and ectodermal cells. (**K,L**) Cell tracks of serosa and amnion cells at subsequent time points of development reveal spreading behavior at the anterior extraembryonic anlage and illustrate that the anterior amnion is formed almost exclusively from cells lateral to the serosa anlage anterior of the cephalic furrow. Embryos and close-ups (**A-I,K,L**) are shown with anterior left. Scale bars, 10 µm.

Figure 2 – figure supplement 1. Analysis of embryonic development was based on a total of 12 MuVi-SPIM recordings (**A**). (**B-E**) To register embryonic development within and between species, the dynamics of the initial, fast phase of germband extension were used as reference (Rauzi et al., 2015); M.abdita wildtype (**B**, n=3), M.abdita zen RNAi (**C**, n=4), M.abdita mmp1 RNAi (**D**, n=3) and D.melanogaster wildtype (**E**, n=2).

Figure 3. The lateral amnion of *M.abdita* forms a ventrally open epithelium. (**A,B**) Cells of the lateral amnion were identified during serosa disjunction (**A**); their position was tracked until mid-germband retraction (**B**). (**C,C'**) Stills from time-lapse recordings illustrate how the amnion "flips back" and starts migrating towards the dorsal midline, exposing filamentous protrusions towards the dorsal side of the embryo. Relative positions of amnion (red arrow)

and a basal actin cable of the amnion (white arrow head) are indicated. (**D,E**) Dynamics of filamentous cell protrusions are visualized by two-color images displaying different time points (first time point cyan, second time point green). (**F-G'**) Expression of a late amnion marker gene (*Mab-egr*) reflects amnion behavior observed by in vivo F-actin staining and cell tracking. Protrusions are indicated with black arrowheads.

Figure 4. Formation of a supracellular actin cable at the serosa boundary. (**A**,**A'**) Accumulation of F-actin at the interface of amnion and serosa cells during germband extension stage. (**B-C**) Supracellular actin cable leads serosa spreading (**B**,**B'**) and serves as marker for serosa expansion. Separation of serosa from amnion is indicated (yellow line) (**C**). (**D,D'**) Selected time points from *in toto* recordings illustrate how serosa "flips over" the adjacent amnion, which in turn folds under the serosa and exposes a baso-lateral membrane with filamentous protrusions towards the basal serosa membrane. Relative positions of amnion (red arrow) and leading actin cable of the serosa (white arrow head) are indicated.

Figure 5. Serosa tissue spreading is active, involves cell oscillations, and increases after detachment from the amnion. (**A-C**) Expansion of the serosa occurred in two phases, i.e. before (**A,A'**) and after (**A'',A'''**) the separation from adjacent and underlying tissues. Serosa separated from adjacent tissue first at its anterior, then posterior, and finally lateral boundaries (**B**). The main expansion is homogenous and occurred at a constant rate, excluding beginning and ventral closure (**C**). (**D-E'**) Disjunction of the serosa was preceded by a 30-minute interval of negligible area increase (grey in C), during which increased local oscillation in cell area occurred in cells away from (**D,D'**) but not at the actin cable boundary (**E,E'**). (**F,G**) To compare the closure speed of the serosa window in *M.abdita* with dorsal closure in D.melanogaster (Hutson et al., 2003), distances were measured between the serosa fronts along the ventral midline (width: W) and along the equator (height: H) over time, starting shortly after the serosa had spread over the anterior and posterior poles. Linear fits were used to extract an estimate of the closure speeds for two serosal closure events. Both fronts closed in a linear fashion, with a mean v_W of 12.7 and v_H of 2.9 µm/s. Closure along the midline was at least three times faster than the corresponding process of dorsal closure in *D.melanogaster* and suggests zippering-independent tissue fusion.

Figure 6. Extraembryonic cell and tissue dynamics in dorsal amnion and amnioserosa. (**A-D'**) The experimental transformation of the serosa into an amnion in *Mab-zen* RNAi embryos results in the loss of epithelial spreading (**A-C**) and a loss of cell oscillation (**D,D'**). (**F**) Loss of these serosa specific properties coincides with an early, yet retarded germband retraction. (**F-I'**) The evolutionary transformation of serosa and amnion into a single dorsal amnioserosa coincides with a loss of epithelial spreading (**F-H**), while serosa-specific cellular properties like apical oscillation remain (**I-I'**). (**J**) The dynamics of germband retraction in *D.melanogaster* are more similar to *M.abdita* wildtype than to Mab-zen RNAi embryos.

Figure 7. Loss of ECM remodeling enzyme activity affects extraembryonic and embryonic morphogenesis in flies. (**A**) Expression of Mab-mmp1 during germband extension stage. (**B-D**) Expression of the M.abdita serosa marker Mab-ddc during germband extension stage in wildtype (**B**), Mab-mmp1 RNAi (**C**), and Mab-mmp1 CRISPR/Cas9 embryos (**D**). (**E-I**) Knockdown of Mab-mmp1 increases the dorsal tissue compression and delays serosa/amnion disjunction (**E-G**), but it does not affect serosa cell behavior (**H,H'**) and the dynamics of germband retraction (**I**).

Video 1. The amnion in *M.abdita* remains a ventrally open epithelium until after the onset of germband retraction. SPIM time-lapse recording of a Megaselia embryo; cell outline revealed by Lifeact-mCherry injected as recombinant protein at syncytial blastoderm stage. Shown is an unrolled ventrolateral surface view, indicating a ventrally open epithelium until after germband retraction completed. Anterior is to the left, dorsal is up.

Video 2. 3D cut corresponding to video 1. Shown is the amnion layer before and after the onset of germband retraction (at 300 minutes). Along the anterior-to-posterior axis of the embryo, the video frame has been centered on the same set of cells, thus eliminating most movements resulting from the retracting germband. Anterior is to the left, dorsal is up.

Video 3. The serosa in *M.abdita* folds over and then separates from the amnion. SPIM time-lapse recording of a lateral surface view. Note that when the serosa spreads over the adjacent amnion, the actin cable follows as the amnion folds underneath the serosa. Along the dorsal-to-ventral circumference of the embryo, the video frame of the unrolled surface encompasses the lateral midline of the embryo. Anterior is to the left, dorsal is up.

Video 4. 3D cut corresponding to video 3. Shown is the serosa layer before and at serosa-amnion disjunction (at 135 minutes). Along the anterior-to-posterior axis of the embryo, the video frame has been kept at constant absolute position because of little movements in the germband. Anterior is to the left, dorsal is up.

Video 5. The serosa in *M.abdita* develops from a dorsal blastoderm domain and envelopes the complete embryo. Time-lapse recording of a lateral *in toto* view of serosa development; Anterior is to the left, dorsal is up. Anterior is to the left, dorsal is up.

Video 6. Identical to video 5, the manually tracked serosa is tinted. Anterior is to the left, dorsal is up.

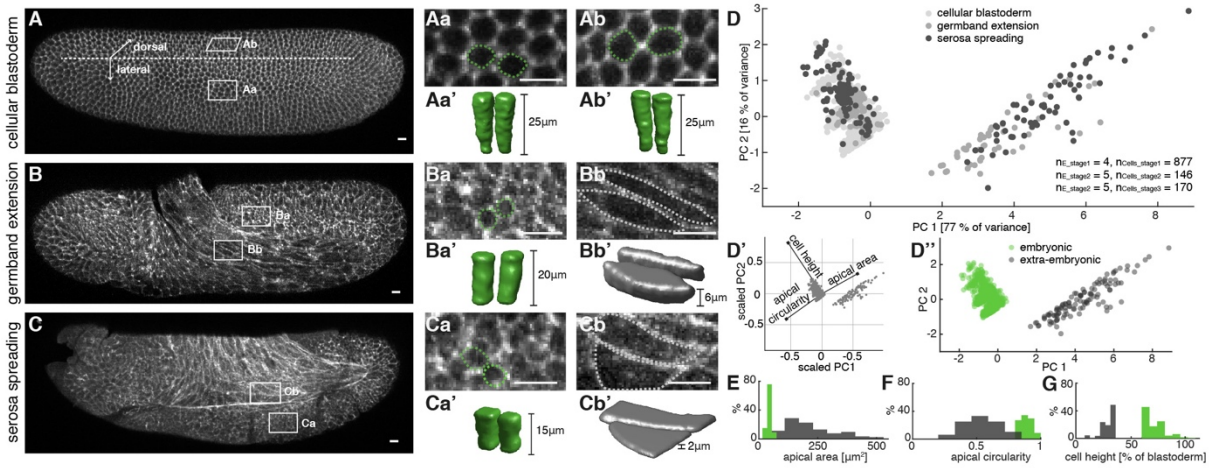

Figure 1.

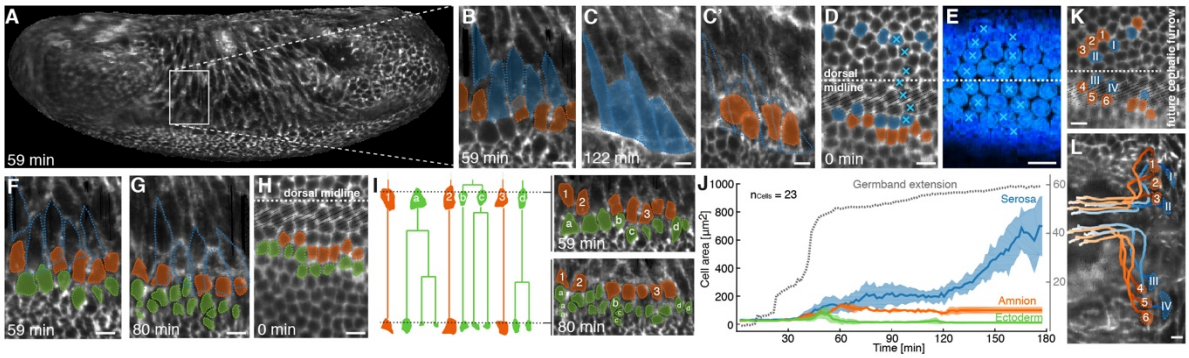

Figure 2.

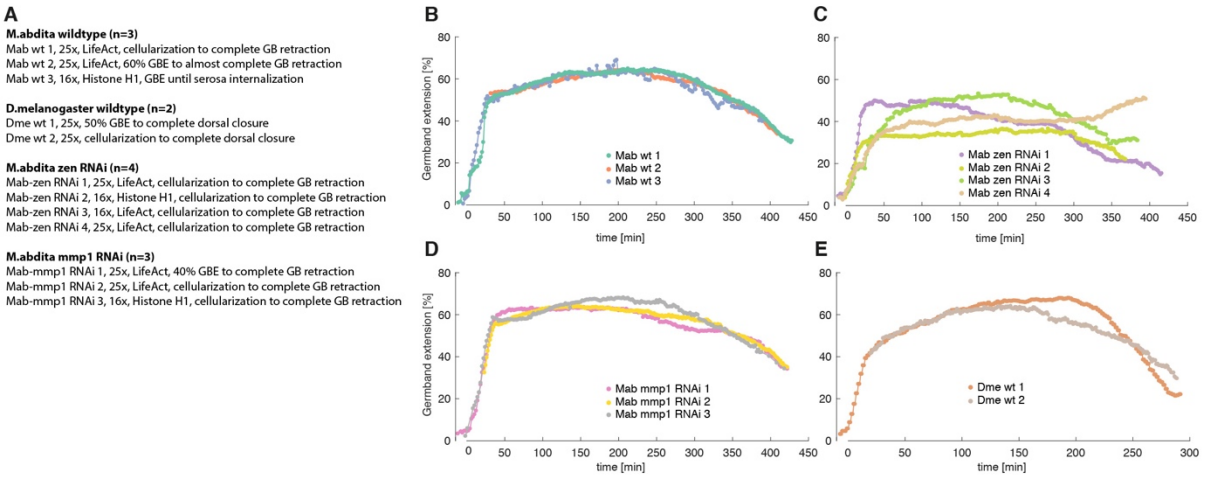

Figure 2 – figure supplement 1.

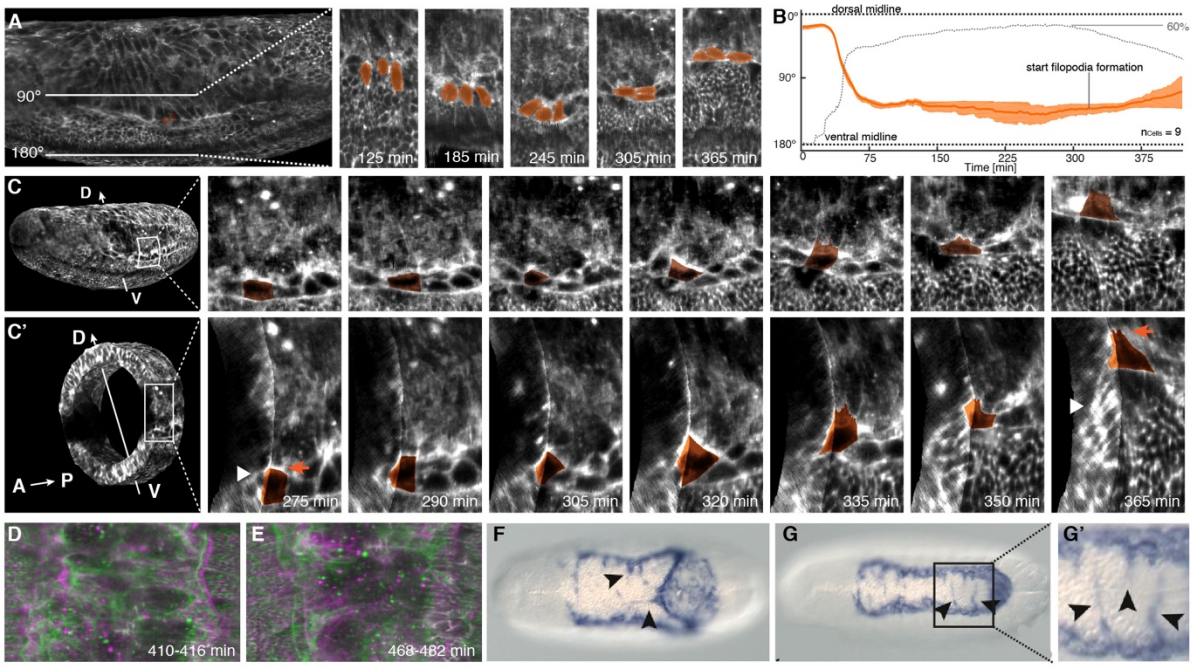

Figure 3.

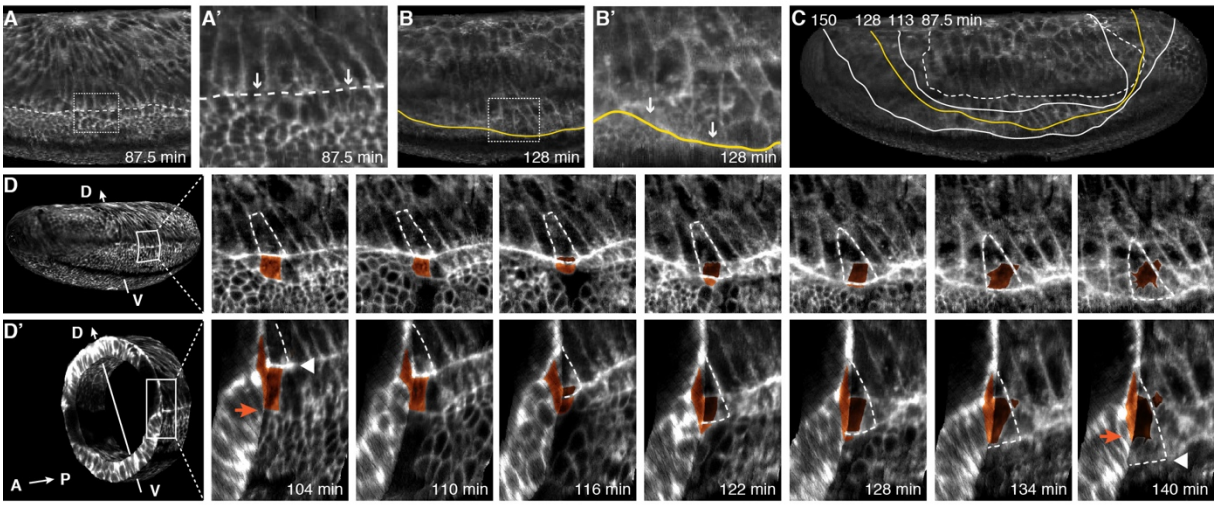

Figure 4.

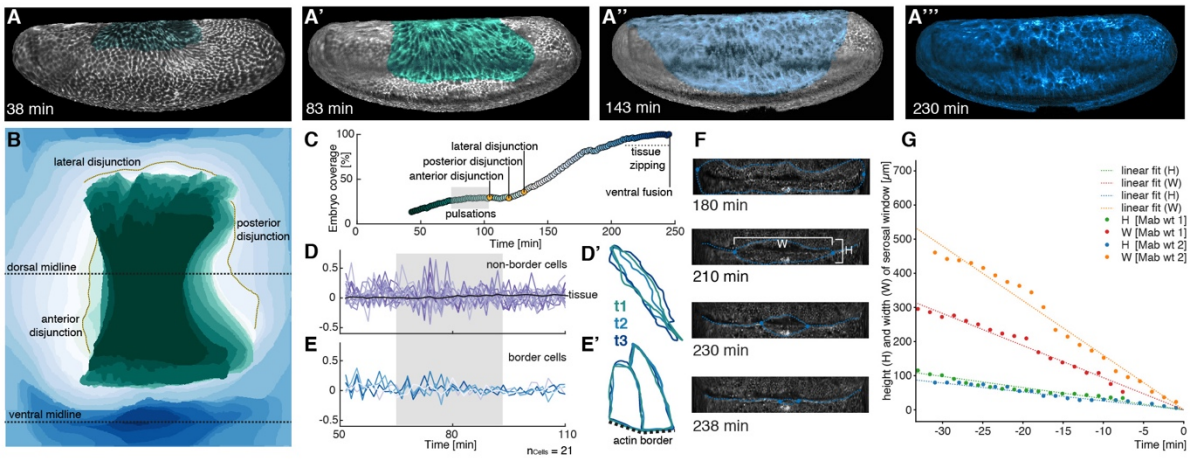

Figure 5.

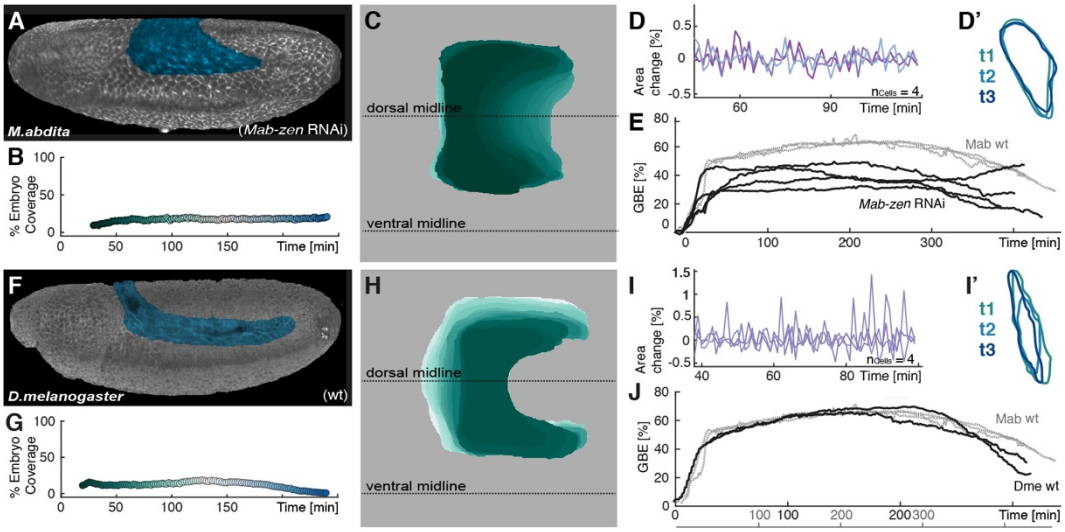

Figure 6.

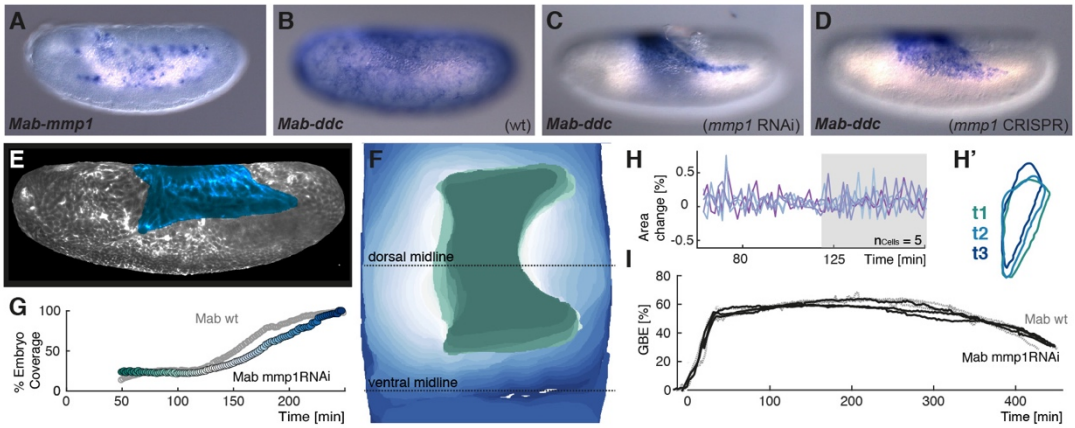

Figure 7.